**Climate
of the Past
Discussions**

Strength of forest-albedo feedback in mid-Holocene climate simulations

J. Otto[1,2,*], T. Raddatz[1], and M. Claussen[1,3]

[1]Max Planck Institute for Meteorology, Hamburg, Germany
[2]International Max Planck Research School on Earth System Modelling, Hamburg, Germany
[3]Meteorological Institute, University Hamburg, KlimaCampus, Germany
[*]now at: LSCE, Laboratoire des Sciences du Climat et l'Environnement, CEA-CNRS-UVSQ,
UMR8212, Gif-Sur-Yvette, France

Correspondence to: J. Otto (juliane.otto@lsce.ipsl.fr)

Title Page	
Abstract	Introduction
Conclusions	References
Tables	Figures
◄◄	►►
◄	►
Back	Close
Full Screen / Esc	
Printer-friendly Version	
Interactive Discussion	

Full Screen / Esc

Abstract

Reconstructions of the mid-Holocene climate, 6000 years before present, suggest that spring temperatures were higher at high northern latitudes compared to the pre-industrial period. A positive feedback between expansion of forest and climate persum-
5   ably contributed to this warming. In the presence of snow, forests have a lower albedo than grass land. Therefore the expansion of forest likely favoured a warming in spring, counteracting the lower insolation at the mid-Holocene.

We investigate this vegetation-climate interaction under mid-Holocene forcing with a comprehensive general circulation model (ECHAM5/JSBACH). We performed two
10   sets of model simulations with either weak or strong reduction in surface albedo by snow-covered forest. The setup of simulations allowed us to calculate the pure contribution by the vegetation-climate interaction to the climate signal. Compared to the set with weak snow masking, the simulations with strong snow masking prevail a three times higher spring warming by 0.34 °C north of 60° N. The additional gain of forest is
15   only 13%.

We show that the parameterisation of the albedo of snow leads to uncertainties in the temperature signal but does not explain the strong spring warming suggested by previous simulations. We rather suggest that studies with coarser resolved representation of vegetation than in ECHAM5/JSBACH overestimated the increase in forest at
20   the mid-Holocene and thus the strength of the vegetation climate.

1   Introduction

Most temperature reconstructions indicate that during the mid-Holocene (about 6000 years before present) temperatures were on average higher compared to the pre-industrial period at high northern latitudes. On average, the climate north of 60° N was
25   ∼ 1.0 °C warmer in summer, ∼ 1.7 °C in winter, and ∼ 2.0 °C in the annual mean in comparison to the pre-industrial climate (Sundqvist et al., 2010a,b). It is striking that the

reconstructed annual mean temperature is higher than the winter and summer temperature. Sundqvist et al. (2010a) propose that the mid-Holocene spring and autumn temperatures may have been considerably higher than in the reconstructed winter and summer temperatures.

Higher temperatures during autumn have likely be caused by the stronger mid-Holocene insolation at early autumn (Berger, 1978). Higher temperatures during spring, however, cannot be explained by the insolation signal as the high northern latitudes received less insolation during mid-Holocene spring compared to the pre-industrial period. This leads to the assumption that some feedbacks between the land surface and atmosphere may have caused warmer springs during the mid-Holocene.

In fact, there exists a strong feedback between snow-covered land and the climate as snow covered forest has a lower albedo than snow-covered lower vegetation. Trees protrude the snow layer and hence decrease the high albedo of snow (Otterman et al., 1984). Additionally, vegetation reconstructions for the mid-Holocene show that forest cover increased and expanded to the north. In Northwestern Canada and Northern Eurasia, the treeline advanced near to the Arctic coastline and reached its northern most position of the Holocene period (MacDonald et al., 2000). Presumably, the warmer conditions during mid-Holocene summer favoured the growth of forest, which led to a decrease in albedo during the cold season and favoured warmer temperatures in spring which reinforced the growth of forest (Claussen, 2004).

Studies with climate models corroborate the assumption of higher mid-Holocene spring temperatures by this positive vegetation-climate feedback. Foley et al. (1994) have performed simulations with an atmosphere-ocean general circulation model (GCM) and prescribed an exaggerated extent of mid-Holocene forest. In their study the increase in forest yields a warming of approximately $4.00\,^\circ\text{C}$ north of $60\,^\circ\text{N}$ during spring. Wohlfahrt et al. (2004) also used an atmosphere-ocean GCM but coupled this asynchronously with a vegetation model. They simulated for the mid-Holocene a polward shift of boreal forest cover and an expansion in mid-latitude grasslands. Compared to simulated vegetation cover under modern orbital forcing, the expanded

forest led to a springtime warming of 0.95 °C north of 40° N. Two mid-Holocene studies with synchronously coupled atmosphere-ocean-vegetation GCMs revealed a weaker spring warming: Gallimore et al. (2005) presented a spring warming of ∼ 0.40 °C north of 60° N, the study by Otto et al. (2009b) revealed an even weaker warming of 0.08 °C
5   north of 60° N.

The discrepancy between the different model results may be related to the usage of different models and parameterisations. Previous work has revealed that the albedo values of snow-covered surfaces vary strongly among the suite of GCMs used in the Fourth Assessment Report of the Intergovernmental Panel on Climate Change (Meehl
10   et al., 2007). The range of albedo values in the models is shown to have a direct impact on the spread in projections of climate change over the continental interior of North America (Hall et al., 2008). Thus, we assume that the spread of albedo values may also lead to a spread of temperature signals in simulations of mid-Holocene climate. To test this assumption, we investigate how much the parameterisation of the albedo of snow-
15   covered forest influences the strength of the feedback between the forest and climate and hence the magnitude of the spring warming under mid-Holocene forcing. For this purpose, we determine the pure contribution of the vegetation-climate interaction to the mid-Holocene climate signal with two different sets of simulations: a) simulations with a relatively weak reduction of albedo of snow by forest, and b) simulations with
20   a relatively strong reduction of the albedo of snow by forest.

2   The albedo scheme in JSBACH

We performed this study with the MPI-ESM which consists of ECHAM5 (Roeckner et al., 2003), including the land surface scheme JSBACH (Raddatz et al., 2007) with a dynamic vegetation module (Brovkin et al., 2009).
25   The albedo scheme in JSBACH computes the temporal and spatial changes of the land-surface albedo (see Appendix A). It provides a spatially explicit surface albedo calculation for the near infrared (NIR) as well as for the visible range (VIS).

In general, the albedo is calculated separately for surfaces covered by green leaves and covered by soil. If the land surface is snow covered, the albedo of a snow-covered fraction of the grid box and the albedo of snow-covered forest canopies is additionally computed. A detailed description of the albedo calculation in JSBACH is given in the
5   Appendix B.

We performed two sets of simulations. The first set of simulations was performed with a weak reduction of the albedo of snow by forest. We call this reduction of the albedo of snow "the strength of snow masking" (δ_α) defined as the difference between the albedo of grass and forest which is higher than 0.1 only in the presence of snow. The strength
10 of snow masking depends on the type of forest, wether deciduous or evergreen forest is used. In the set of simulations with a weak strength of snow masking, particularly deciduous forest has a small effect on the albedo of snow because of the loss of its foliage during the cold season.

The second set of simulations is performed with an enhanced snow masking by for-
15 est, in particular by deciduous forest. In general, the calculation of the albedo depends on the leaf area index (LAI) which determines how much of the fraction is shaded by the canopy (see Appendix B). As during winter LAI of deciduous forest is very low, Roesch and Roeckner (2006) suggested to introduce a stem area index to replace LAI for deciduous trees in winter. When deciduous trees have lost their needles or
20 leaves, this stem area index mimics the stem and branches shadowing the ground below the canopy. The current parameterisation includes a stem area index set to 1 which introduces a weak snow masking for deciduous forest (Fig. 1). To account for a stronger snow masking by deciduous forest, we set the stem area index to 3. In addition, we introduce a stronger snow masking by evergreen forest by reducing the albedo
25 of snow-covered canopy from $\alpha_{\text{snow,c}} = 0.25$ to $\alpha_{\text{snow,c}} = 0.20$ (Sturm et al., 2005) and we increased the minimum albedo of snow for bare lands in the near infrared from $\alpha_{\text{snow,nir}} = 0.3$ to $\alpha_{\text{snow,nir}} = 0.4$.

Title Page

Abstract | Introduction

Conclusions | References

Tables | Figures

◄ | ►►

◄ | ►

Back | Close

Full Screen / Esc

Printer-friendly Version

Interactive Discussion

2.1 The simulation protocol

In total, we performed 8 simulations (see Table 1): four simulations with weak snow masking and four simulations with strong snow masking. All simulations were run with atmospheric CO_2-concentrations set to 280 ppm and with the same sea-surface
5 temperature and sea-ice cover prescribed as monthly values. To ensure statistically robust results (Otto et al., 2009a), we simulated 250 years for the atmosphere-only runs and 480 years for the atmosphere-vegetation runs and considered the last 240 years of all experiments for the analysis.

In this study, the term "vegetation-climate interaction" (see Eqs. 1 and 2) comprises
10 all interactions between vegetation and atmosphere, and determines the pure contribution of this interaction to the mid-Holocene climate signal. Four simulations are required to calculate the pure contribution of the vegetation-climate interaction (ΔV_w for weak snow masking and ΔV_s for strong snow masking) to the mid-Holocene climate signal (Stein and Alpert, 1993): two simulations with dynamic vegetation, one
15 with pre-industrial ($0k(AV)_w$ and $0k(AV)_s$) and one with mid-Holocene orbital forcing ($6k(AV)_w$ and $6k(AV)_s$). The two corresponding atmosphere-only simulations had the vegetation prescribed from the $0k(AV)_w$-simulation and $0k(AV)_s$-simulation, respectively, and were run with pre-industrial and mid-Holocene orbital forcing. To calculate the pure contribution of the vegetation-climate interaction ΔV_w and ΔV_s, we have to
20 compare the results of the two simulations with the vegetation run interactively with the two atmosphere-only simulations :

$$\Delta V_w = (6k(AV)_w - 0k(AV)_w) - (6kA_w - 0kA_w) \tag{1}$$

$$\Delta V_s = (6k(AV)_s - 0k(AV)_s) - (6kA_s - 0kA_s) \tag{2}$$

The pure contribution ΔV_w and ΔV_s can be evaluated for all climate parameters. If we
25 consider a specific climate parameter, for example the air temperature [T], we use the symbol $\Delta V_w[T]$ and $\Delta V_s[T]$, respectively.

In order to keep the definition of seasons consistent with insolation forcing in pre-industrial and mid-Holocene climate, an astronomically based calendar is necessary (Joussaume and Braconnot, 1997). Accordingly, we considered the spring season defined by the astronomical dates: vernal equinox and summer solstice. Since an astro-
5 nomical calendar is not implemented in our model, we calculated all spring values from the daily output according to the model's astronomical parameters for pre-industrial and for mid-Holocene climate, respectively (Timm et al., 2008; Otto et al., 2009b). In previous mid-Holocene studies, seasons have been determined by monthly means which were computed with the present-day calendar. To compare our results with previous
10 studies we shifted the seasons backwards by three weeks relative to the astronomical season. Seasonal averages are then computed from the daily output of the model for the pre-industrial and the mid-Holocene period, respectively.

3 Snow-masking parameterisations

A strong reduction in surface albedo by forest emerges solely with the presence of
15 snow. This effect is mostly confined to the land north of 50° N as seen in Fig. 1a, b. The figures show the simulated snow cover just before the melting season at the Northern Hemisphere. Considering the parameterisation with weak snow masking, the albedo of snow covered land is much more effectively reduced by evergreen forest than by deciduous forest (Fig. 1c, e). Albedo of grassland is up to 0.65 lower than
20 the albedo of evergreen forest, whereas this albedo reduction is limited to 0.30. In the simulations performed with strong snow masking, the maximum strength of snow masking by evergreen forest is increased by 0.05 and covers a larger area than with the weak snow masking simulations. The strength of snow masking by deciduous forest is increased by almost a factor of two due to the larger stem area index. The strength
25 ranges from 0.1 to 0.5 and is strongest in the region between 55–70° N.

The albedo of snow can be measured by aircraft and satellite, remote sensing and ground observations (e.g., Essery et al., 2009; Barlage et al., 2005; Jin et al., 2002;

Betts and Ball, 1997). These measurements demonstrate that the albedo of snow is strongly variable and depends on various factors like for example the type of snow, weather conditions, size of sample area (Moody et al., 2007). Hence, the estimates for the strength of the snow masking vary in the literature between 0.1 (Jin et al., 2002) and 0.6 (Essery et al., 2009). All studies agree on that evergreen forest masks the albedo of snow more effectively than deciduous forest.

In general, the simulated strength of the snow masking in JSBACH is in both parameterisations in agreement with observed snow masking. With the simulated weak snow masking at lower end and the simulated strong snow masking of evergreen forest at the upper end, the parameterisations in JSBACH cover the range of observed strength of snow masking.

4 Simulated vegetation-climate interaction

Our study focuses on springtime as the forest-albedo feedback is expected to be strongest in this season (Hall and Qu, 2006; Dery and Brown, 2007). The reason for this is that in spring both snow extent and incoming solar radiation are relatively large compared to autumn and winter.

The experiments with weak snow masking yield a spring warming of 0.12 °C (Table 2) for the land north of 60° N. The positive temperature anomaly is largest in the circumpolar belt between 60–70 °C (Fig. 3a). The temperature increases locally up to 0.60 °C. The simulations with strong snow masking result in higher spring temperatures. The warming is most pronounced in Eastern Siberia. Here the forest expansion increases the temperature by up to 1.3 °C (Fig. 3b). Averaged over the land region north of 60° N, the temperature increase is 0.34 °C, and hence is almost three times higher than with the weak snow masking.

The basis for a strong vegetation-climate interaction during the mid-Holocene is the expansion of forest. As reconstructions indicate, the tree line was shifted further north to the Arctic coast line (MacDonald et al., 2000). Both simulation sets produce this forest expansion for the region north of 60° N (Fig. 2). The simulations with weak snow

masking result in an forest increase by $11.29 \times 10^5\,\mathrm{km}^2$, the simulations with strong snow masking yield a 13% stronger increase by $12.71 \times 10^5\,\mathrm{km}^2$. The forest expansion comprises both the increase in evergreen and deciduous forest but in varying degree. Evergreen forest increases in Northern Europe, North-Western Siberia, and Northern Canada. The simulations with strong snow masking result in a $2 \times 10^5\,\mathrm{km}^2$ larger expansion of evergreen forest and $0.56 \times 10^5\,\mathrm{km}^2$ smaller expansion of deciduous forest relative to the simulations with weak snow masking.

The set of simulations with strong snow masking reduces the surface albedo more strongly than with weak snow masking (Fig. 3c, d). In the belt between 60–70° N , the surface albedo is almost everywhere reduced up to -0.14 compared to -0.08 in the experiment with weak snow masking. In this latitudinal belt, the net surface solar radiation is increased compared to the pre-industrial period in both experiments (Fig. 3e, f). In North-Eastern Siberia occurs the maximum raise of net surface solar radiation with $12\,\mathrm{W\,m}^{-2}$, compared to $1\,\mathrm{W\,m}^{-2}$ due to only changes in the orbital parameters, in the set of simulations with strong snow masking. This is more than twice the radiation which is available at surface in the set of simulations with weak snow masking. In both experiments the patterns of albedo reduction and the increase in net surface solar radiation follow roughly the patterns of forest increase (Fig. 2).

It is striking that only the simulations with strong snow masking show a lower snow depth in spring compared to the pre-industrial period (Fig. 3g, h). Snow is reduced in a slightly larger region than in the region where forest increase (Fig. 2 c–f). The snow depth decreases regionally up to 15 mm, in particular in the regions with strongest expansion in deciduous forest. In the experiment with weak snow masking the reduction in snow depth does not exceed 5 mm and occurs only in the region of strongest forest increase.

To investigate the forest-albedo feedback more closely, we analyse the variability of the seasonal cycle (Fig. 4). Figure 4a reveals that in both experiments the temperature anomaly is not constant in spring. With the increase of insolation after winter, temperature rises until it reaches its maximum ($\Delta V_{\mathrm{w}}[T] = 0.37$, $\Delta V_{\mathrm{s}}[T] = 0.67$) and declines

Back | Close

Full Screen / Esc

Printer-friendly Version

Interactive Discussion

during the rest of the year. The experiment with weak snow masking shows at the beginning of mid-Holocene lower spring air-temperatue than in the pre-industrial period. In the experiment with strong snow masking, air-temperature is in winter already higher compared to the pre-industrial temperature.

5 Surface albedo is in both experiments considerably lower throughout winter and spring $\Delta V_w[\alpha] = \sim -2\%$, $\Delta V_s[\alpha] = \sim -3.5\%$) relative to the pre-industrial period. However, only the low albedo (Fig. 4c) in the experiment with strong snow masking leads to a considerable increase in surface solar radiation ($\Delta V_s[S] = 2.7\,\mathrm{W\,m^{-2}}$) (Fig. 4b). This favours the warming of near-to surface air in spring, leading to a strong melting of snow
10 (Fig. 4d). The surface albedo in the experiment with weak snow masking is not as low as in the simulations with strong snow masking. The consequence is that less radiation is absorbed to warm the air and to effectively melt snow. Hence, the feedback between snow-covered forest and atmosphere is not as strong as in the experiment with strong snow masking, resulting in lower spring temperatures.

15 As the snow masking by forest is in the simulations with low snow masking too weak to considerably warm spring air, we want to test if the expansion of forest and its snow masking are actually the main land components that drive the vegetation-climate interaction. We compare the simulated net surface downward radiation signal $\Delta V_w[S]$ with a simple estimate of the change in net surface solar radiation (δS_{est}) due to the
20 strength of snow masking and the change in forest. We multiply the solar downward radiation of $0kAw$ by the strength of the snow masking for evergreen and deciduous forest, respectively, (see Fig. 1 c–f) and by the change in forest for evergreen and deciduous forest, respectively, between the mid-Holocene and pre-industrial simulations ($\Delta(AV)_w$) and average this product for the spring season:

25 $$\delta S_{est} = \int_{t_1}^{t_2} S \downarrow (\delta\alpha_e \cdot \Delta f_e + \delta\alpha_d \cdot \Delta f_d)dt/(t_2 - t_1) \qquad (3)$$

where $S \downarrow$ is the solar downward radiation in $\mathrm{W\,m^{-2}}$ for $0k$, $\delta\alpha_e$ is the strength of snow masking of evergreen forest, $\delta\alpha_d$ is the strength of snow masking of deciduous forest,

Δf_e the change in evergreen forest fraction and Δf_d the change in deciduous forest fraction between $6k$ and $0k$, and t_1 represents the date of the beginning of spring and t_2 the date of the end of spring.

Figure 5 shows the estimated net surface solar radiation δS_{est} with the simulated net surface solar radiation $\Delta V_w[S]$. The patterns of change in net surface solar radiation are very similar. However, δS_{est} reveals a stronger increase in net surface solar radiation compared to the simulated net surface solar radiation by about a factor of two. In addition, δS_{est} does not produce the reduction in net surface solar radiation of the region over North America between 40–60° N and North-East Europe. We can support the statement that in our model the expansion of forest and its snow masking are the main land components that drive of the vegetation-climate interaction (Otterman et al., 1984; Harvey, 1988).

The deviation of the estimated net surface solar radiation δS_{est} from the simulated net surface solar radiation $\Delta V_w[S]$ indicates that the net surface solar radiation is weakened by a process which is not included in the simple estimate (Eq. 3). This process could be an increase in cloud fraction due to the fact that trees have a more productive canopy than grass and shrubs and therefore, transpire more water (Pielke and Vidale, 1995; Eugster et al., 2000; Beringer et al., 2005). Possibly, this increase in transpiration favours an increase in cloud fraction (Table 2) and thus counteracts the warming. In both experiments, the sensible and the latent flux increases (Table 2). We cannot derive from these set of simulations if this increase is caused by the expansion of forest, nor can we derive that the increase in total cloud fraction is the only process which weakens the net surface solar radiation.

5 Comparison with previous studies

Proxies of the mid-Holocene climate give information about winter, summer and annual mean temperatures and the vegetation distributions, e.g. the position of the northern tree line.

To test our model how well it can reproduce mid-Holocene climate derived from proxies, we compare our simulations with available data sets. With both sets of simulations, we simulate much lower temperatures in winter ($\Delta(AV)_\mathrm{w} = -0.04\,^\circ\mathrm{C}$, $\Delta(AV)_\mathrm{s} = 0.01\,^\circ\mathrm{C}$) and in the annual mean ($\Delta(AV)_\mathrm{w} = 0.24\,^\circ\mathrm{C}$, $\Delta(AV)_\mathrm{s} = 0.35\,^\circ\mathrm{C}$) compared to the reconstructions (winter: $\sim 1.70\,^\circ\mathrm{C}$, annual: $\sim 2.00\,^\circ\mathrm{C}$, respectively (Sundqvist et al., 2010a,b). For summer, ECHAM5/JSBACH overestimates the mid-Holocene warming by almost $1\,^\circ\mathrm{C}$ ($\Delta(AV)_\mathrm{w} = 1.82\,^\circ\mathrm{C}$, $\Delta(AV)_\mathrm{s} = 1.97\,^\circ\mathrm{C}$) compared to reconstructed summer temperature of only $\sim 1.00\,^\circ\mathrm{C}$ (Sundqvist et al., 2010a,b).

The mismatch between the model simulations and reconstructions has likely several reasons: (1) The simulations were performed without dynamic ocean and thus neglected important interactions between ocean, land and atmosphere (Otto et al., 2009a). (2) The reconstructed temperature values are an unweighted average over the region north of 60° N (Sundqvist et al., 2010a). (3) The average of the reconstructed temperature depend on the uncertainty in individual reconstructions and the number of sites. For example, the sparsity of winter temperature reconstructions make the estimated change in winter less reliable than the reconstructed summer and annual mean temperatures (Sundqvist et al., 2010a).

Reconstructions of the mid-Holocene treeline suggest an asymmetric response of the vegetation to the change in insolation (MacDonald et al., 2000; Bigelow et al., 2003). The reconstructions show northward shifts of forest by up to 200 km in Central Siberia, and 50–100 km in Western Europe and in North-West Canada. For Eastern Canada, reconstruction suggest that the tree line was further south than present. The simulated northward extension in forest area for the mid-Holocene is in general agreement with the reconstructions (see Fig. 2). The increase in deciduous forest in Eastern Siberia is also supported by reconstructions (Texier et al., 1997). Wohlfahrt et al. (2008) presented an evaluation of GCM simulations of the mid-Holocene with palaeovegetation data. In their study, the different GCMs simulate an increase in forest between $6–16 \times 10^5\,\mathrm{km}^2$ north of 60° N. Our results with an increase in forest between $11.29–12.71 \times 10^5\,\mathrm{km}^2$ are in the range of the results by Wohlfahrt et al. (2008).

Full Screen / Esc

Printer-friendly Version

Interactive Discussion

In contrast to our simulated spring warming, previous studies suggest a stronger contribution of the vegetation-climate interaction to the mid-Holocene climate signal. Simulations with the EMIC CLIMBER-2 by Ganopolski et al. (1998) exhibit a warming of up to 2.5 °C (60–70° N) in winter by the vegetation-climate interaction due to a strong
5 forest expansion in their mid-Holocene simulations. Ganopolski et al. (1998) obtained a factor of three more increase in forest than we simulated. This strong warming of the vegetation-climate interaction and the large expansion of forest is corroborated by Crucifix et al. (2002). Their study, performed with the EMIC MoBidiC, produces a very strong warming of 5 °C north of 60° N in spring and an expansion of forest by about
10 a factor of four more than we simulated. However, the authors refer to this strong expansion of forest and warming as unrealistic.

Simulations with GCMs reveal a weaker contribution of the vegetation-climate interaction than simulated with EMICs. A study (Gallimore et al., 2005) with the GCM FOAM-LPJ produces a vegetation-climate interaction of 0.40 °C. Gallimore et al. (2005)
15 explain this weak warming with a large mid-latitude expansion of grass cover outweighing the expansion in boreal forest cover in their model and therefore weakening the vegetation-climate interaction. This is not the case in our model as we do not simulate an expansion of grass in the mid-latitudes. Wohlfahrt et al. (2004) coupled the vegetation model BIOME1 asynchronously with the GCM IPSL. Their simulations show
20 a spring warming that reaches 0.95 °C averaged over the region north 40° N with an expansion of forest only half of our simulated increase in forest.

We suggest that the spread in simulated springtime temperature for the mid-Holocene can be partly explained by the way vegetation is treated in the respective climate model. In comparison to the study by Wohlfahrt et al. (2004), we use a GCM
25 including a fully coupled vegetation module. The vegetation module follows a tiling approach (Brovkin et al., 2009), so that on each of the model's grid boxes, a mosaic of different vegetation types can exist. The vegetation composition is temporally variable and derived from succession processes such as establishment and mortality. Wohlfahrt et al. (2004), however, used a vegetation module asynchronously coupled with a GCM.

Forest-albedo feedback in mid-Holocene

J. Otto et al.

Title Page

Abstract | Introduction

Conclusions | References

Tables | Figures

◄ | ►

◄ | ►

Back | Close

Full Screen / Esc

Printer-friendly Version

Interactive Discussion

In their approach, each grid box contained only one vegetation type. With a climate change, a whole grid box changes, for example to forest, whereas with the tiling approach only a fraction of the grid box is turned into forest. The temperature response to large-scale changes is stronger compared to the fractional change in vegetation cover in MPI-ESM. The same applies for studies with EMICs which are performed in a much coarser resolution compared to our study (3.75° at the meridian). Commonly, EMICs distinguish only between two vegetation types (trees and grass) per grid box with a resolution of 10° in latitude and 51° in longitude (Ganopolski et al., 1998). A grid box of this size covers a larger region with either grass or forest than in JSBACH. When the climate changes, for instance due to mid-Holocene insolation forcing, the vegetation cover of each grid box adapts to it and, thus, causes a stronger increase in e.g. forest than simulated with our higher-resolved vegetation model.

Qu and Hall (2007) showed that EMICs tend to present higher albedo values under snowy conditions than more complex models, which explicitly take into account the influence of vegetation on the albedo (e.g. snow masking by forest). Models with a very simple surface-albedo parameterisation tend to have unrealistic strong snow-albedo feedback Qu and Hall (2007). Studies with a forest reflectance model emphasise the need to model the albedo of snow-covered forest more explicitly (Manninen and Stenberg, 2009). For example, snow on the canopy of trees increases the total forest albedo, especially in the red band.

6 Conclusions

We show that the simulated magnitude of spring warming depends on the parameterisation of the albedo of snow. With a doubling of the strength of snow masking, spring warming is increased by a factor three. This temperature increase goes along with an additional gain of total forest of only 13%.

As discussed by Claussen (2009), it is still a challenge to draw a clear conclusion regarding the magnitude of the vegetation-climate interaction. With our model setup

ECHAM5/JSBACH we support the suggestion (Braconnot et al., 2007), that the magnitude of the vegetation-climate interaction is smaller than previously discussed.

We argue that the strength of the vegetation-climate interaction likely depends on how vegetation is represented in a model and its coupling to the climate. Modelling processes more explicitly relative to previous studies as for example continuous shift of vegetation by the tiling approach (Brovkin et al., 2009), the climate-vegetation interaction appears to be weaker.

To support this conclusion, simulations with the same model in different resolutions would be helpful. In the same way, a similar study as presented here with another GCM including a dynamic vegetation model would allow a better understanding of the magnitude of the vegetation-climate interaction.

Appendix A

Maps of leaf albedo and soil albedo

For each PFT a specific albedo of the canopy (green leaves) α_{leaf} is given for visible (VIS) and near-infrared (NIR) range (Table A1). These values are derived from two map of α_{leaf} for each of the spectral bands. The soil albedo, α_{soil}, is read in as two maps (VIS and NIR) at the beginning of each experiment. The four maps of α_{leaf} and α_{soil} have been caluulated from the sensor Moderate-Resolution Imaging Spectroradiometer (MODIS) (Schaaf et al., 2002) reflectance data in a manner similar to Rechid et al. (2008).

The maps of α_{leaf} and α_{soil} are derived by linear regression of the fraction of absorbed photosynthetically active radiation fapar(t) on total surface albedo $\alpha(t)$. Both data sets, fapar(t) and $\alpha(t)$, are based on measurements taken by MODIS aboard the TERRA satellite in the years 2001–2004. Here we use the white sky albedo of VIS and NIR range included in the product MOD43C1, which specifies the albedo on a 0.05 degree grid in 16 day periods. White sky albedo (also referred to as bi-hemispherical

Full Screen / Esc

Printer-friendly Version

Interactive Discussion

reflectance) is the reflectance of a surface under diffuse illumination (same radiance for all viewing directions). It is considered to be a good proxy of the daily average albedo, which is the decisive parameter in the context of climate modelling. Only at high latitudes it slightly underestimates albedo as the solar zenith angle is large throughout the whole day.

The fapar data are taken from the product MOD15A2, which provides 8 day fapar composites on a 1 km sinussoidal grid. Both, albedo and fapar, data sets are remapped to a 0.25° grid excluding pixels with snow cover and the fapar fields are averaged over the 16 day periods of the albedo data set.

The linear regression is done separately for the visible range (incl. UV radiation, 0.3–0.7 µm) and the NIR range (0.7–3 µm) in the following way:

$$\alpha(t) = \text{fcover}(t)\alpha_{\text{leaf}} + (1 - \text{fcover}(t))\alpha_{\text{soil}} \tag{A1}$$

Here fcover(t) is the fraction of the grid box covered by a green canopy. For the visible range it can be approximately assumed that $\text{fcover}(t) = \text{fapar}(t)/(1 - \alpha_{\text{leaf}})$. This implies that the difference in the reflectivity of UV radiation and the photosynthetically active radiation (i.e. the visible radiation) has no substantial influence on the total reflectivity as well as that the radiation reflected at the soil beneath the canopy and penetrating the canopy thereafter is negligible.

$$\alpha_{\text{vis}}(t) = \frac{\text{fapar}(t)}{1 - \alpha_{\text{leaf,vis}}}\alpha_{\text{leaf,vis}} + \left(1 - \frac{\text{fapar}(t)}{1 - \alpha_{\text{leaf,vis}}}\right)\alpha_{\text{soil,vis}} \tag{A2}$$

The coefficients a and b of the linear relation $\alpha_{\text{vis}}(\text{fapar}) = a \times \text{fapar} + b$ are specified by the linear regression of fapar on α_{vis}, so that $\alpha_{\text{leaf,vis}}$ and $\alpha_{\text{soil,vis}}$ can be calculated:

$$\alpha_{\text{vis}}(\text{fapar} = 0) = b = \alpha_{\text{soil,vis}} \tag{A3}$$
$$\alpha_{\text{vis}}(\text{fapar} = 1) = a + b$$
$$= \frac{1}{1 - \alpha_{\text{leaf,vis}}}\alpha_{\text{leaf,vis}} + (1 - \frac{1}{1 - \alpha_{\text{leaf,vis}}})\alpha_{\text{soil,vis}}$$

Title Page

Abstract | Introduction

Conclusions | References

Tables | Figures

◄ | ►

◄ | ►

Back | Close

Full Screen / Esc

Printer-friendly Version

Interactive Discussion

$$\implies \alpha_{\text{leaf,vis}} = \frac{a+b}{1+a} \tag{A4}$$

After $\alpha_{\text{leaf,vis}}$ and $\alpha_{\text{soil,vis}}$ have been determined by linear regression, also $\alpha_{\text{leaf,nir}}$ and $\alpha_{\text{soil,nir}}$ are calculated similarly according to the equation:

$$\alpha_{\text{nir}}(t) = \frac{\text{fapar}(t)}{1-\alpha_{\text{leaf,vis}}} \alpha_{\text{leaf,nir}} + \left(1 - \frac{\text{fapar}(t)}{1-\alpha_{\text{leaf,vis}}}\right) \alpha_{\text{soil,nir}} \tag{A5}$$

5   The albedo values $\alpha_{\text{soil,vis}}$, $\alpha_{\text{leaf,vis}}$, $\alpha_{\text{soil,nir}}$, and $\alpha_{\text{leaf,nir}}$ are used for the calculation of the albedo in JSBACH (see Appendix B).

Appendix B

Albedo calculation in JSBACH

10   The surface albedo of each gridbox in JSBACH is calculated in several steps. Each land gridbox is subdivided into tiles, which represent different PFTs. For these tiles the albedo, α_i, is calculated. The albedo values of all tiles are then weighted by their fractional cover, f_i, and summed to a gridbox average albedo. This is done separately for VIS (wavelength 0.3–0.7 µm) and NIR (0.7–3.0 µm). Finally, the albedo values are

15   passed to the atmospheric model ECHAM5 to be used in the radiation routine.

The albedo of each tile, α_i, is calculated from the albedo of the canopy (green leaves), α_{leaf} (Appendix A), the albedo of soil, α_{soil} (Appendix A), the albedo of snow covered soil α_{snow} and the albedo of snow covered forest canopies $\alpha_{\text{snow,c}}$. The albedo of each tile is calculated for VIS and NIR but to simplify the equations we omit the

20   subscript vis and nir.

The albedo of snow, α_{snow}, is temperature-dependent. It decreases linearly with surface temperature, ranging from a minimum value at the melting point ($\alpha_{\text{snow,vis}} = 0.5$, $\alpha_{\text{snow,nir}} = 0.3$, in the simulation with strong snow masking set to $\alpha_{\text{snow,nir}} = 0.4$) to a maximum value for temperatures of less than $-5\,°C$ ($\alpha_{\text{snow,vis}} = 0.9$, $\alpha_{\text{snow,nir}} = 0.7$).

Title Page

Abstract | Introduction

Conclusions | References

Tables | Figures

|◄ | ►|

◄ | ►

Back | Close

Full Screen / Esc

Printer-friendly Version

Interactive Discussion

The albedo of snow-covered canopy is set to either $\alpha_{snow,c} = 0.25$ or for the set of simulations with strong snowmasking to $\alpha_{snow,c} = 0.20$.

If the vegetation type is grass or shrub, snow on the soil is assumed to also cover the leaves. The albedo of a tile, α_i, which is covered by either grass or shrubs is aggregated as follows. The snow covered fraction of the soil is $f_{snow,s}$, and the fraction of each gridbox, which is free of any vegetation is f_{bare}.

$$\alpha_i = (f_{bare} + (1 - f_{bare})e^{-LAI_i/2})(1 - f_{snow,s})\alpha_{soil} +$$
$$(1 - f_{bare})(1 - e^{-LAI_i/2})(1 - f_{snow,s})\alpha_{leaf} + f_{snow,s}\alpha_{snow} \tag{B1}$$

The first line of Eq. (B1) represents the albedo of the area which is neither covered by leaves nor by snow, the second line the albedo of the area covered by green leaves, and the third line the albedo of snow-covered soil. Whereas for forests the snow on the canopy as well as the masking of snow on the soil by the canopy are considered:

$$\alpha_i = (f_{bare} + (1 - f_{bare})e^{-(LAI_i + stem)/2})((1 - f_{snow,s})\alpha_{soil} + f_{snow,s}\alpha_{snow}) +$$
$$(1 - f_{bare})(e^{-LAI_i/2} - e^{-(LAI_i + stem)/2})((1 - f_{snow,c})\alpha_{soil} + f_{snow,c}\alpha_{snow,c}) +$$
$$(1 - f_{bare})(1 - e^{-LAI_i/2})((1 - f_{snow,c})\alpha_{leaf} + f_{snow,c}\alpha_{snow,c}) \tag{B2}$$

The first line of Eq. (B2) represents the albedo of the area which is not covered by vegetation (green leaves), the second line gives the albedo of the area covered by stems and branches (stem) and the third line the albedo of area which is covered by green leaves. A stem area index of 1 for all forest types is introduced, in particular to account for the snow masking of deciduous forest. In the set of simulations with strong snow masking, the stem area index is set to 3.

A summary of how the albedo of the different surfaces is aggregated, is illustrated in Fig. B1.

References

Barlage, M., Zeng, X. B., Wei, H. L., and Mitchell, K. E.: A global 0.05 degrees maximum albedo dataset of snow-covered land based on MODIS observations, Geophys. Res. Lett., 32, L17405, doi:10.1029/2005GL022881, 2005. 815

Berger, A.: Long-term variations of daily insolation and quaternary climatic changes, J. Atmos. Sci., 35, 2362–2367, 1978. 811

Beringer, J., Chapin, F. S., Thompson, C. C., and McGuire, A. D.: Surface energy exchanges along a tundra-forest transition and feedbacks to climate, Agr. Forest Meteorol., 131, 143–161, 2005. 819

Betts, A. K. and Ball, J. H.: Albedo over the boreal forest, J. Geophys. Res., 102, 28901–28909, 1997. 816

Bigelow, N. H., Brubaker, L. B., Edwards, M. E., Harrison, S. P., Prentice, I. C., Anderson, P. M., Andreev, A. A., Bartlein, P. J., Christensen, T. R., Cramer, W., Kaplan, J. O., Lozhkin, A. V., Matveyeva, N. V., Murray, D. F., McGuire, A. D., Razzhivin, V. Y., Ritchie, J. C., Smith, B., Walker, D. A., Gajewski, K., Wolf, V., Holmqvist, B. H., Igarashi, Y., Kremenetskii, K., Paus, A., Pisaric, M. F. J., and Volkova, V. S.: Climate change and Arctic ecosystems: 1. Vegetation changes north of 55 degrees N between the last glacial maximum, mid-Holocene, and present, J. Geophys. Res., 108, 8170, 2003. 820

Braconnot, P., Otto-Bliesner, B., Harrison, S., Joussaume, S., Peterchmitt, J.-Y., Abe-Ouchi, A., Crucifix, M., Driesschaert, E., Fichefet, Th., Hewitt, C. D., Kageyama, M., Kitoh, A., Loutre, M.-F., Marti, O., Merkel, U., Ramstein, G., Valdes, P., Weber, L., Yu, Y., and Zhao, Y.: Results of PMIP2 coupled simulations of the Mid-Holocene and Last Glacial Maximum – Part 2: feedbacks with emphasis on the location of the ITCZ and mid- and high latitudes heat budget, Clim. Past, 3, 279–296, doi:10.5194/cp-3-279-2007, 2007. 823

Brovkin, V., Raddatz, T., Reick, C. H., Claussen, M., and Gayler, V.: Global biogeo-physical interactions between forest and climate, Geophys. Res. Lett., 36, L07405, doi:10.1029/2009GL037543, 2009. 812, 821, 823

Claussen, M.: The global climate, Chapt. A.4, in: Vegetation, Water, Humans and the Cli-mate: a New Perspective on an Interactive System, edited by: Kabat, P., Claussen, M., Dirmeyer, P. A., Gash, J. H. C., Guenni, L., Meybeck, M., Pielke, R. A., Vörösmarty, C. J., and Lütkemeier, S., Springer-Verlag, Heidelberg, 2004. 811

Claussen, M.: Late Quaternary vegetation-climate feedbacks, Clim. Past, 5, 203–216, doi:10.5194/cp-5-203-2009, 2009. 822

Crucifix, M., Loutre, M. F., Tulkens, P., Fichefet, T., and Berger, A.: Climate evolution during the Holocene: a study with an Earth system model of intermediate complexity, Clim. Dynam., 19, 43–60, 2002. 821

Dery, S. J. and Brown, R. D.: Recent Northern Hemisphere snow cover extent trends and implications for the snow-albedo feedback, Geophys. Res. Lett., 34, L22504, doi:10.1029/2007GL031474, 2007. 816

Essery, R., Rutter, N., Pomeroy, J., Baxter, R., Stahli, M., Gustafsson, D., Barr, A., Bartlett, P., and Elder, K.: An evaluation of forest snow process simulations, B. Am. Meteorol. Soc., 90, 1120–1135, 2009. 815, 816

Eugster, W., Rouse, W. R., Pielke, R. A., McFadden, J. P., Baldocchi, D. D., Kittel, T. G. F., Chapin, F. S., Liston, G. E., Vidale, P. L., Vaganov, E., and Chambers, S.: Land-atmosphere energy exchange in Arctic tundra and boreal forest: available data and feedbacks to climate, Glob. Change Biol., 6, 84–115, 2000. 819

Foley, J. A., Kutzbach, J. E., Coe, M. T., and Levis, S.: Feedbacks between climate and boreal forests during the Holocene epoch, Nature, 371, 52–54, 1994. 811

Gallimore, R., Jacob, R., and Kutzbach, J.: Coupled atmosphere-ocean-vegetation simulations for modern and mid-Holocene climates: role of extratropical vegetation cover feedbacks, Clim. Dynam., 25, 755–776, 2005. 812, 821

Ganopolski, A., Kubatzki, C., Claussen, M., Brovkin, V., and Petoukhov, V.: The influence of vegetation-atmosphere-ocean interaction on climate during the mid-Holocene, Science, 280, 1916–1919, 1998. 821, 822

Hall, A. and Qu, X.: Using the current seasonal cycle to constrain snow albedo feedback in future climate change, Geophys. Res. Lett., 33, L03502, doi:10.1029/2005GL025127, 2006. 816

Title Page

Abstract | Introduction

Conclusions | References

Tables | Figures

◄ | ►

◄ | ►

Back | Close

Full Screen / Esc

Printer-friendly Version

Interactive Discussion

Hall, A., Qu, X., and Neelin, J. D.: Improving predictions of summer climate change in the United States, Geophys. Res. Lett., 35, L01702, doi:10.1029/2007GL032012, 2008. 812

Harvey, L. D. D.: On the role of high-latitude ice, snow, and vegetation feedbacks in the climatic response to external forcing changes, Climatic Change, 13, 191–224, 1988. 819

5 Jin, Y. F., Schaaf, C. B., Gao, F., Li, X. W., Strahler, A. H., and Zeng, X. B.: How does snow impact the albedo of vegetated land surfaces as analyzed with MODIS data?, Geophys. Res. Lett., 29, 1374, 2002. 815, 816

Joussaume, S. and Braconnot, P.: Sensitivity of paleoclimate simulation results to season definitions, J. Geophys. Res., 102, 1943–1956, 1997. 815, 838

10 MacDonald, G. M., Velichko, A. A., Kremenetski, C. V., Borisova, O. K., Goleva, A. A., Andreev, A. A., Cwynar, L. C., Riding, R. T., Forman, S. L., Edwards, T. W. D., Aravena, R., Hammarlund, D., Szeicz, J. M., and Gattaulin, V. N.: Holocene treeline history and climate change across Northern Eurasia, Quaternary Res., 53, 302–311, 2000. 811, 816, 820

Manninen, T. and Stenberg, P.: Simulation of the effect of snow covered forest floor on the total
15 forest albedo, Agr. Forest Meteorol., 149, 303–319, 2009. 822

Meehl, G., Stocker, T., Collins, W. D., Friedlingstein, F., Gaye, A., Gregory, J., Kitoh, A., Knutti, R., Murphy, J., Noda, A., Raper, S., Watterson, I., Weaver, A., and Zhao, Z.-C.: Global climate projections, in: Climate Change 2007: The Physical Science Basis, Contribution of Working Group I to the Fourth Assessment Report of the Intergovernmental Panel on Climate
20 Change, edited by: Solomon, S., Qin, D., Manning, M., Chen, Z., Marquis, M., Averyt, K. B., Tignor, M., and Miller, H. L., Cambridge University Press, Cambridge, United Kingdom and New York, NY, USA, 2007. 812

Moody, E. G., King, M. D., Schaaf, C. B., Hall, D. K., and Platnick, S.: Northern Hemisphere five-year average (2000–2004) spectral albedos of surfaces in the presence of snow: statistics
25 computed from Terra MODIS land products, Remote Sens. Environ., 111, 337–345, 2007. 816

Otterman, J., Chou, M. D., and Arking, A.: Effects of nontropical forest cover on climate, J. Clim. Appl. Meteorol., 23, 762–767, 1984. 811, 819

Otto, J., Raddatz, T., and Claussen, M.: Climate variability-induced uncertainty in mid-
30 Holocene atmosphere-ocean-vegetation feedbacks, Geophys. Res. Lett., 36, L23710, doi:10.1029/2009GL041457, 2009a. 814, 820

Otto, J., Raddatz, T., Claussen, M., Brovkin, V., and Gayler, V.: Separation of atmosphere-ocean-vegetation feedbacks and synergies for mid-Holocene climate, Geophys. Res. Lett.,

36, L09701, doi:10.1029/2009GL037482, 2009b. 812, 815, 838

Pielke, R. A. and Vidale, P. L.: The boreal forest and the polar front, J. Geophys. Res.-Atmos., 100, 25755–25758, 1995. 819

Qu, X. and Hall, A.: What controls the strength of snow-albedo feedback?, J. Climate, 20, 3971–3981, 2007. 822

Raddatz, T. J., Reick, C. H., Knorr, W., Kattge, J., Roeckner, E., Schnur, R., Schnitzler, K. G., Wetzel, P., and Jungclaus, J.: Will the tropical land biosphere dominate the climate-carbon cycle feedback during the twenty-first century?, Clim. Dynam., 29, 565–574, 2007. 812

Rechid, D., Raddatz, T., and Jacob, D.: Parameterization of snow-free land surface albedo as a function of vegetation phenology based on MODIS data and applied in climate modelling, Theor. Appl. Climatol., 95, 245–255, 2008. 823

Roeckner, E., Bäuml, G., Bonaventura, L., Brokopf, R., Esch, M., G., Giorgetta, M., Hagemann, S., Kirchner, I., Kornblueh, L., Manzini, E., Rhodin, A., Schlese, U., Schulzweida, U., and Tompkins, A.: The atmospheric general circulation model ECHAM5, Part I: Model description, Tech. Rep. Rep. 349, Max Planck Institute for Meteorology, available from: MPI for Meteorology, Bundesstr. 53, 20146 Hamburg, Germany, 127 pp., 2003. 812

Roesch, A. and Roeckner, E.: Assessment of snow cover and surface albedo in the ECHAM5 general circulation model, J. Climate, 19, 3828–3843, 2006. 813

Schaaf, C. B., Gao, F., Strahler, A. H., Lucht, W., Li, X. W., Tsang, T., Strugnell, N. C., Zhang, X. Y., Jin, Y. F., Muller, J. P., Lewis, P., Barnsley, M., Hobson, P., Disney, M., Roberts, G., Dunderdale, M., Doll, C., d'Entremont, R. P., Hu, B. X., Liang, S. L., Privette, J. L., and Roy, D.: First operational BRDF, albedo nadir reflectance products from MODIS, Remote Sens. Environ., 83, 135–148, 2002. 823

Stein, U. and Alpert, P.: Factor separation in numerical simulations, J. Atmos. Sci., 50, 2107–2115, 1993. 814

Sturm, M., Douglas, T., Racine, C., and Liston, G. E.: Changing snow and shrub conditions affect albedo with global implications, J. Geophys. Res.-Biogeo., 110, G01004, doi:10.1029/2005JG000013, 2005. 813

Sundqvist, H. S., Zhang, Q., Moberg, A., Holmgren, K., Körnich, H., Nilsson, J., and Brattström, G.: Climate change between the mid and late Holocene in northern high latitudes – Part 1: Survey of temperature and precipitation proxy data, Clim. Past, 6, 591–608, doi:10.5194/cp-6-591-2010, 2010a. 810, 811, 820

Title Page

Abstract | Introduction

Conclusions | References

Tables | Figures

|◄ | ►|

◄ | ►

Back | Close

Full Screen / Esc

Printer-friendly Version

Interactive Discussion

Sundqvist, H. S., Zhang, Q., Moberg, A., Holmgren, K., Körnich, H., Nilsson, J., and Brattström, G.: Corrigendum to "Climate change between the mid and late Holocene in northern high latitudes – Part 1: Survey of temperature and precipitation proxy data" published in Clim. Past, 6, 591–608, 2010, Clim. Past, 6, 739–743, doi:10.5194/cp-6-739-2010, 2010b. 810, 820

Texier, D., de Noblet, N., Harrison, S. P., Haxeltine, A., Jolly, D., Joussaume, S., Laarif, F., Prentice, I. C., and Tarasov, P.: Quantifying the role of biosphere-atmosphere feedbacks in climate change: coupled model simulations for 6000 years BP and comparison with palaeodata for Northern Eurasia and Northern Africa, Clim. Dynam., 13, 865–882, 1997. 820

Timm, O., Timmermann, A., Abe-Ouchi, A., Saito, F., and Segawa, T.: On the definition of seasons in paleoclimate simulations with orbital forcing, Paleoceanography, 23, PA2221, doi:10.1029/2007PA001461, 2008. 815

Wohlfahrt, J., Harrison, S. P., and Braconnot, P.: Synergistic feedbacks between ocean and vegetation on mid- and high-latitude climates during the mid-Holocene, Clim. Dynam., 22, 223–238, 2004. 811, 821

Wohlfahrt, J., Harrison, S. P., Braconnot, P., Hewitt, C. D., Kitoh, A., Mikolajewicz, U., Otto-Bliesner, B. L., and Weber, S. L.: Evaluation of coupled ocean-atmosphere simulations of the mid-Holocene using palaeovegetation data from the Northern Hemisphere extratropics, Clim. Dynam., 31, 871–890, doi:10.1007/s00382-008-0415-5, 2008. 820

Table 1. List of experiment setup and simulations.

Experiment name	Prescribed vegetation cover	Duration (yrs)
ΔV_w		
$6k(AV)_w$	–	480
$0k(AV)_w$	–	480
$6kA_w$	from $0k(AV)_w$	250
$0kA_w$	from $0k(AV)_w$	250
ΔV_s		
$6k(AV)_s$	–	480
$0k(AV)_s$	–	480
$6kA_s$	from $0k(AV)_s$	250
$0kA_s$	from $0k(AV)_s$	250

Table 2. Change in vegetation, desert fraction and climate of the simulations with both weak snow masking (left) and strong snow masking (right). The change in vegetation cover is derived from the simulations with dynamic vegetation. All values are spring mean values and averaged over land over the area 60°–90° N. Please note that fluxes towards the atmosphere (sensible and latent heat fluxes) are negative.

Change in vegetation and desert in 10^5 km^2	$(AV)_w$	$(AV)_s$
Evergreen forest	4.84	6.82
Deciduous forest	6.45	5.89
Grass	−1.68	−1.96
Shrubs	−0.46	0.03
Desert fraction	−9.15	−10.78

Climate change in spring	ΔV_w	ΔV_s
Air-temperatue	0.12	0.34
Surface albedo	−0.02	−0.03
Precipitation (mm season^{-1})	0.28	0.85
Snow depth in (mm)	−0.53	−1.70
Sensible heat flux in W m^{-2}	−0.42	−0.72
Latent heat flux in W m^{-2}	−0.38	−0.69
Net surface solar radiation W m^{-2}	1.05	1.77
Cloud cover fraction	0.002	0.004

Table A1. α_{leaf} values for VIS and NIR for each PFT derived from MODIS data set.

PFT	Albedo VIS	Albedo NIR
Forest tropical evergreen	0.03	0.21
Forest tropical deciduous	0.04	0.23
Forest temperate/boreal evergreen broadleaf	0.05	0.25
Forest temperate/boreal deciduous broadleaf	0.07	0.28
Forest temperate/boreal evergreen needleleaf	0.05	0.26
Forest temperate/boreal deciduous needleleaf	0.05	0.26
Shrubs raingreen	0.05	0.25
Shrubs cold	0.07	0.28
Grass C3	0.08	0.34
Grass C4	0.08	0.34
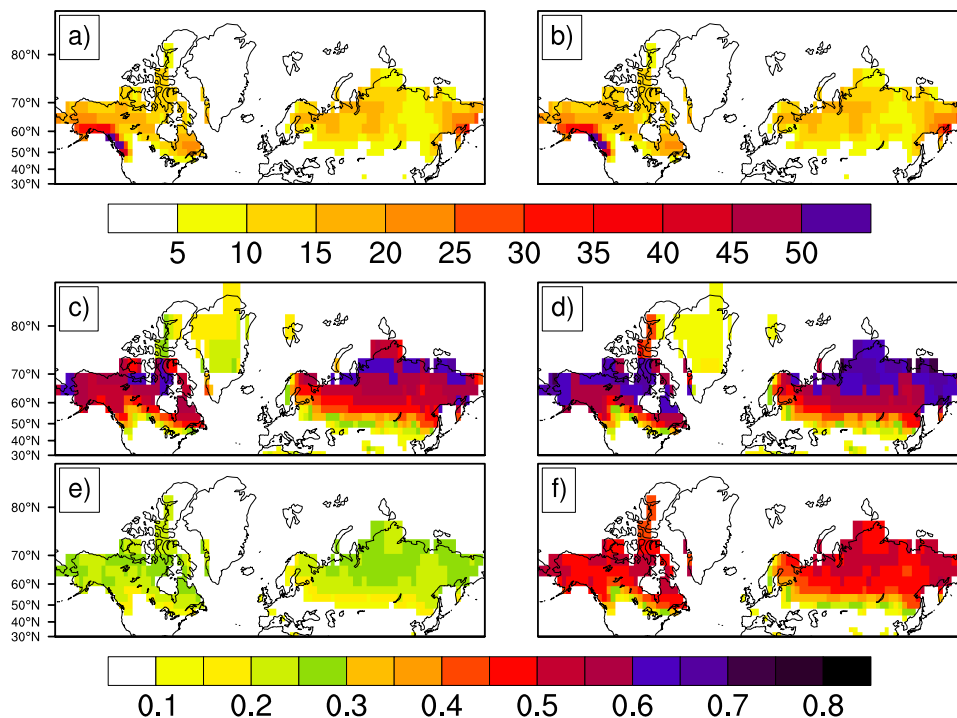
Fig. 1. The upper two panels show the snow depth in cm for March for both the parameterisation with weak snow masking **(a)** and with strong snow masking **(b)**. The panels below show the difference between the albedo of grass (VIS + NIR) and the albedo of forest (VIS + NIR) for March. We refer to this difference as strength of snow-masking (δ_α). The left column shows δ_α for the parameterisation with weak snow masking separately for evergreen forest **(c)** and for deciduous forest **(e)**. The right column shows δ_α for the parameterisation with strong snow masking separately for evergreen forest **(d)** and for deciduous forest **(f)**.
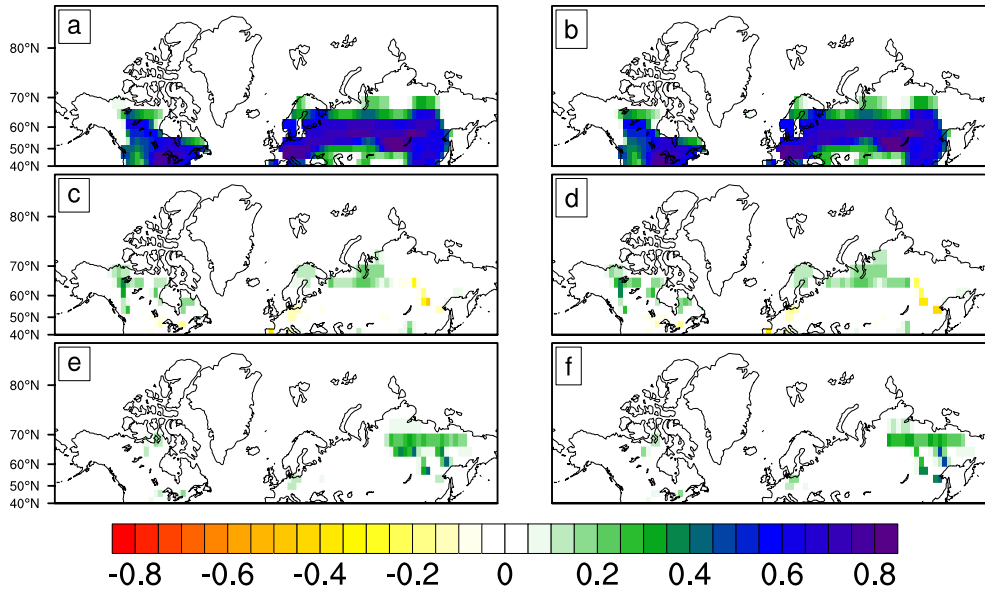
Fig. 2. Forest cover for the two sets of simulations with weak snow masking (left column) and strong snow masking (right column). The upper two panels (**a** and **b**) give the total forest cover for present day climate. The panels **(c)** and **(d)** show the change in evergreen forest $6k - 0k$, the panels **(e)** and **(f)** for deciduous forest $6k - 0k$.
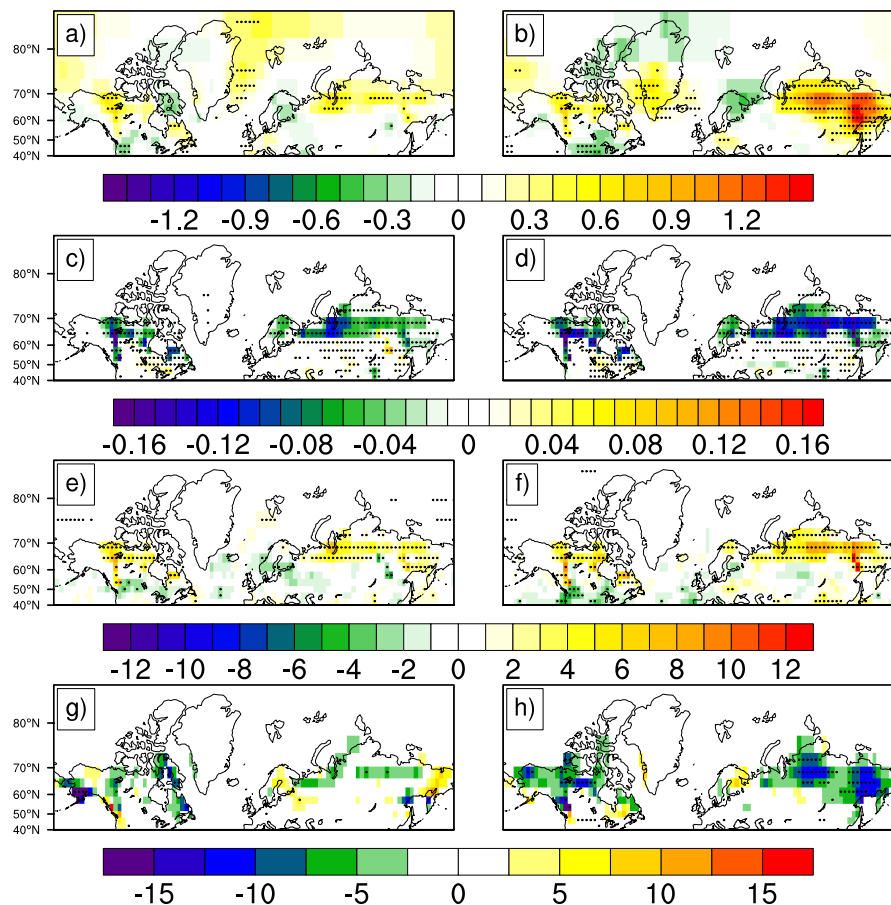
Fig. 3. Mean spring climate values for ΔV_w (left column) and ΔV_s (right column): air-temperature (**a** and **b**) in °C, surface albedo (**c** and **d**), net surface solar radiation in $\mathrm{W\,m^{-2}}$ (**e** and **f**), snow depth in mm (**g** and **h**). The black dots indicate significant values with 0.05 level of significance.
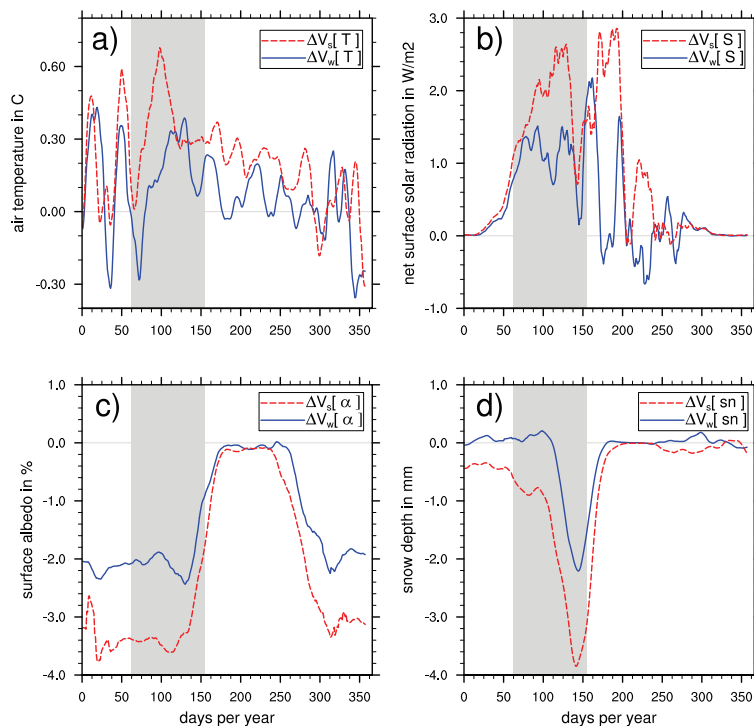
Fig. 4. Seasonal cycle for the simulations with weak snow masking (V_w = blue line) and strong snow masking (V_s = red, dashed line) for the climate variables: air-temperature in °C **(a)**, net surface solar radiation in W m^{-2} **(b)**, surface albedo **(c)** and snow depth in mm **(d)**. The time series are smoothed with a 10-day running mean. Grey shading marks the period define as spring at $6k$. Please note: The comparison between $6k$ and $0k$-simulations cannot be made without caution. Variations of the Earth's orbit change the beginning and end of the seasons (Joussaume and Braconnot, 1997). However, the usage of a modern calendar effects only marginally the climate anomaly in spring (Otto et al., 2009b).
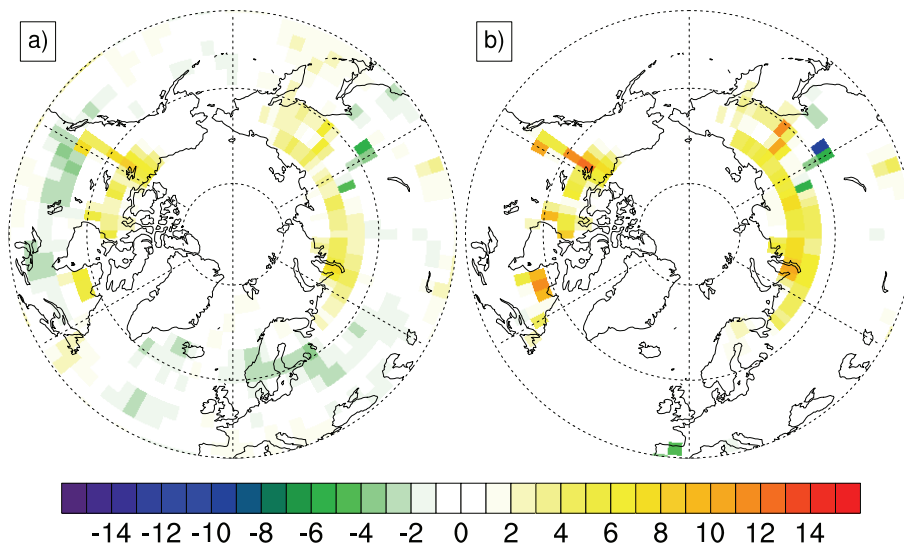
Fig. 5. Spring net surface radiation for $\Delta V_w[S]$ **(a)** with the calculated net surface radiation δS_{est} **(b)** derived from the solar downward radiation for $0k$, the change in forest fraction from $0k$ to $6k$ and the strength of snow masking.
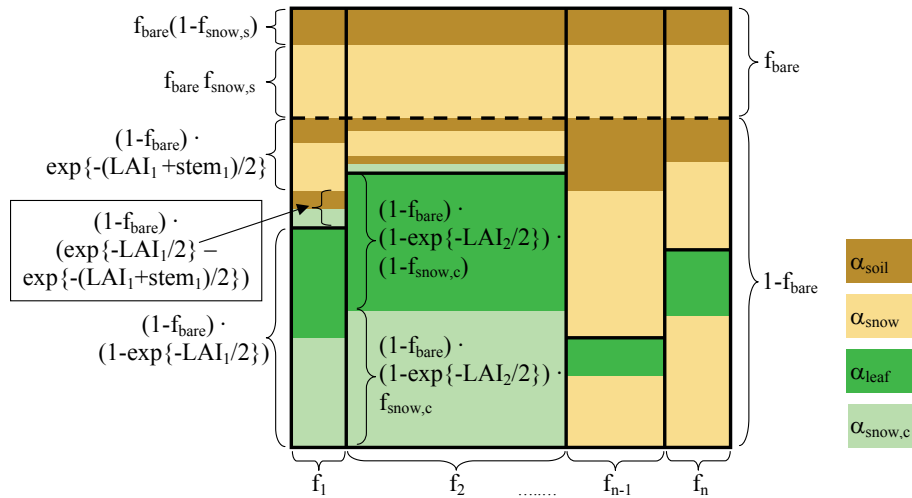
Fig. B1. Illustration of the terms in the Eqs. (B1) and (B2). In this example tile 1 and tile 2 are covered by forest, whereas tile $n-1$ and tile n are occupied by grasses or shrubs.

Title Page

Abstract | Introduction

Conclusions | References

Tables | Figures

|◄ | ►|

◄ | ►

Back | Close

Full Screen / Esc

Printer-friendly Version

Interactive Discussion